JOURNAL OF SOLID STATE CHEMISTRY **134,** 238–247 (1997)
ARTICLE NO. SC977546

# Structural and Local Environment Modifications in a Chemically Lithiated Iron Thiospinel

C. Bousquet, A. Krämer, C. Pérez Vicente, J. L. Tirado,* J. Olivier-Fourcade, and J. C. Jumas[1]

*Laboratoire de Physicochimie de la Matière Condensée (UMR C5617 CNRS), Université de Montpellier II, Place Eugène Bataillon, 34095 Montpellier Cedex 5, France; and * Laboratorio de Química Inorgánica, Facultad de Ciencias, Universidad de Córdoba, Avda. San Alberto Magno s/n, 14004 Córdoba, Spain*

Received May 30, 1997; accepted July 11, 1997

**We present a combined $^{57}$Fe Mössbauer/X-ray diffraction (Rietveld analysis) study carried out on an $In_{16}Fe_8S_{32}$ spinel before and after chemical lithium insertion. To accommodate the new inserted cations in the structure, two mechanisms are observed. First, for a low lithium content, a cation migration takes place from the usually occupied 8*a* and 16*d* sites toward the usually unoccupied 8*b* and 16*c* sites, with distortion of the sulfur coordination polyhedra. Second, for a high lithium content, when both 16*c* and 16*d* octahedral sites are occupied, a decrease of the distortion of the polyhedra is observed. During the insertion process, no clear reduction of Fe atoms is observed but there is an increase in the covalent character of the Fe–S bonds.** © 1997 Academic Press

## INTRODUCTION

Compounds with a spinel-related structure have been widely investigated as host materials for the insertion of small electron-donor atoms. These solids possess a framework lattice that provides a three-dimensional interstitial space for accommodating the inserted elements and remains intact during the insertion process. Lithium insertion properties make spinel materials interesting candidates for applications of technological relevance such as electrodes in lithium and lithium ion batteries (1–6).

The unit formula of spinel compounds is commonly written as $AB_2X_4$. Its space group is $Fd\bar{3}m$. The unit cell of the spinel structure contains 32 cubic close-packed $X$ anions placed in the 32*e* site. Eight cations are tetrahedrally surrounded by four $X$ anions (8*a* site) and sixteen cations are octahedrally coordinated by six anions (16*d* site). In the so-called *normal spinel*, the $A$ cations are placed in the tetrahedral 8*a* site and the $B$ cations in the octahedral 16*d* site. In the *inverse spinel*, the $A$ cations are now randomly placed in the octahedral 16*d* site, half of the $B$ cations are in the tetrahedral 8*a* site, and the rest of the $B$ cations are in the octahedral 16*d* site. The degree of inversion can be described by a parameter $\lambda$, defined as the fraction of $A$ atoms in the octahedral site. For a normal spinel, $\lambda = 0$, and for an inverse spinel, $\lambda = 1$. Intermediate values can also be found, $0 < \lambda < 1$. Moreover, $\lambda$ is not necessarily constant for a given spinel and may show dependence with heat treatment (7).

Post-transition metals of Groups 13 and 14 provide several examples of sulfide compounds having a spinel-related structure. Particularly, indium thiospinels include binary (high-temperature indium sesquisulfide) and ternary ($MIn_5S_8$, $M$ = Cu, Ag; $MIn_2S_4$, $M$ = Mn, Fe, Co, Ni; cation-deficient $SnIn_4S_8$) compounds. Some of them have been previously studied as host materials for lithium insertion (4, 5). $In_2FeS_4$ is a particular case, since for this compound an intermediate value of $\lambda = 0.95$ has been reported (8). However, to our knowledge, the intercalation properties of $In_2FeS_4$ have not been reported until now. Iron thiospinel compounds offer interesting possibilities for a better understanding of the redox insertion process, as the use of $^{57}$Fe Mössbauer spectroscopy gives detailed information on the local environment of iron atoms in the structure.

In this paper, the structural aspects and the local environment of iron atoms present in the spinel structure after chemical lithium insertion (via *n*-butyllithium) are examined by X-ray diffraction (Rietveld analysis) and Mössbauer spectroscopy.

## EXPERIMENTAL

The iron indium thiospinel was prepared by the solid-state reaction between the binary compounds $\beta$-$In_2S_3$ and FeS in 1 : 1 ratio. The mixture was placed into a silica tube and sealed under vacuum ($< 10^{-5}$ Torr). It was heated at 6 K/h until 973 K, maintaining this temperature constant for 10 days. The tube was then quenched in water to obtain the cubic phase.

[1] To whom correspondence should be addressed.



0022-4596/97 $25.00

Chemical lithium insertion was carried out by the *n*-butyllithium technique (6). The sulfide powder was suspended in a 2.5 M solution of ($n$-$C_4H_9$)Li in hexane. A thermostatic bath was used to keep the temperature constant at 309 K. The experimental device was kept under a dry argon atmosphere during the reaction. The treated products were collected, filtered, washed with hexane, and stored in an argon-filled glovebox to avoid oxidation reactions. The lithium content of the samples was obtained by atomic emission spectroscopy on a Philips (Pye Unicam SP9) spectrophotometer.

X-ray powder diffraction patterns (XDP) were recorded on a Philips diffractometer using Cu$K\alpha$ radiation. To avoid the oxidation reactions of the lithiated products during the recording of the XDP, the samples were covered with Parafilm. To analyze the structural modifications induced by the intercalation process, Rietveld analyses of XDP were carried out with the aid of the computer program "Rietveld Analysis Program DBWS-9411" (9).

$^{57}$Fe Mössbauer spectra were recorded at room temperature in the constant-acceleration mode on an ELSCINT-AME40 spectrometer. The velocity scale was calibrated with the magnetic sextet spectrum of a high-purity iron foil absorber. The source was $^{57}$Co(Rh). Recorded spectra were fitted to Lorentzian profiles by the least-squares method (10) and the fit quality controlled by the classical $\chi^2$ and misfit test.

## RESULTS AND DISCUSSION

### *(a) Pristine $In_{16}Fe_8S_{32}$*

The XDP of pristine $In_{16}Fe_8S_{32}$ was characteristic of a single-phase product and could be indexed in a spinel-related cubic system. A Rietveld analysis confirmed the spinel structure with the $Fd\bar{3}m$ space group. The structural fitted parameters are included in Table 1. The unit cell parameter $a = 10.6076$ Å is in good agreement with previously reported data (11). The value of $\lambda$ obtained from the refined cation distribution was 0.910, which is close to that previously reported by Hill *et al.* (8), $\lambda = 0.95$. Figure 1 shows the experimental XDP, the refinement results, and the difference between them.

**TABLE 1**
**Results of the Rietveld Analysis of XDP Data of $In_{16}Fe_8S_{32}$**

| Space group: $Fd\bar{3}m$, $a = 10.6076(2)$ Å, $x = 0.2569(3)$ | | | | |
|---|---|---|---|---|
| | | Occupancy | | |
| Site | Coordinates | In | Fe | S |
| 8*a* ($T_d$) | (1/8, 1/8, 1/8) | 7.28(4) | 0.72(4) | |
| 16*d* ($O_h$) | (1/2, 1/2, 1/2) | 8.72(4) | 7.28(4) | |
| 32*e* | ($x$, $x$, $x$) | | | 32.00 |
| Correlation Factors | | | | |
| $R_p$ | $R_{wp}$ | $R_{expected}$ | $S = R_{wp}/R_{exp}$ | $R_{Bragg}$ |
| 7.00 | 9.19 | 8.10 | 1.13 | 2.61 |

**TABLE 2**
**Hyperfine Parameters of Mössbauer Spectrum of $In_{16}Fe_8S_{32}$: Isomer Shift (IS), Quadrupole Splitting (QS), Full-Width at Half-Maximum (LW), and Relative Area (RA)**

| Site | IS (mm/s) | QS (mm/s) | LW (mm/s) | RA (%) |
|---|---|---|---|---|
| 16*d* ($O_h$) | 0.864(1) | 3.2(1) | 0.325(8) | 93(1) |
| 8*a* ($T_d$) | 0.66(5) | 0.94(5) | 0.58(6) | 7(1) |

Figure 2 shows the transition $^{57}$Fe spectrum of $In_{16}Fe_8S_{32}$. It consists of two paramagnetic quadrupole-split doublets with marked differences in the hyperfine parameters (Table 2). This result is in good agreement with previous studies (11). First-row transition metal indium sulfides have a partially inverse distribution with the metal ions in both tetrahedral and octahedral sites (8, 12). Thus, the doublet with the larger quadrupole splitting can be unambiguously ascribed to $Fe^{2+}$ ions in octahedral 16*d* sites, while the second doublet in the central part of the spectrum is due to $Fe^{2+}$ ions in tetrahedral 8*a* sites. The larger linewidth of the second subspectrum can be explained by a superposition of several contributions corresponding to different environments of tetrahedral sites (11). From integration of the two doublets, the octahedral-Fe/total-Fe ratio (equivalent to the previously defined $\lambda$) was found to be 0.93, a value which is close to that obtained from the Rietveld analysis, 0.91. The good correspondence between the values confirms the intermediate cation distribution on this compound.

### *(b) Lithiated Samples*

Figure 3 shows the evolution of the amount of inserted lithium by the *n*-butyllithium technique as a function of the reaction time. From this plot, it is evident that the maximum insertion rate is observed between 20 and 30 h under the conditions described in the experimental section.

$^{57}$Fe Mössbauer spectroscopy and Rietveld analysis of XPD data were used to obtain complementary information about the lithium insertion mechanism in terms of lattice expansion, cation distribution, etc. Due to the complex possibilities emerging from the large number of sites available for lithium insertion and the possible redistribution of transition metal ions, it was not possible to start the analysis from a prefixed model of site occupancy. Thus, a first refinement was carried out for all the lithiated samples by assuming that the two cations (In and Fe) could partially occupy all the available tetrahedral (8*a*, 8*b*, and 48*f*) and octahedral

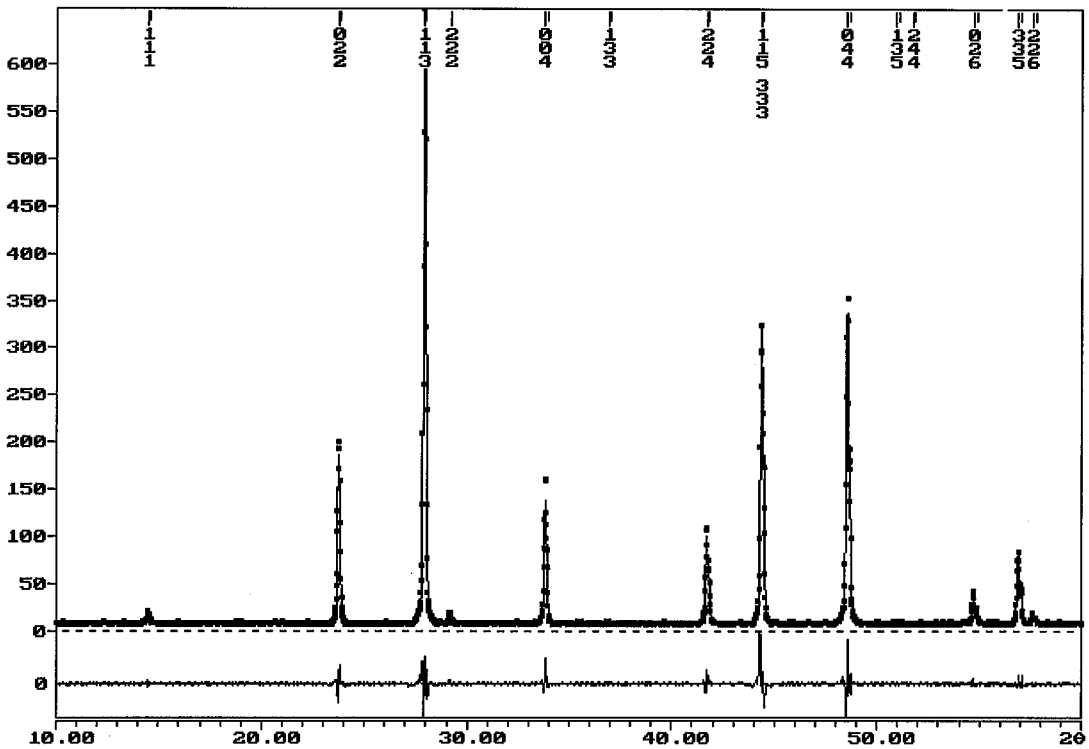


**FIG. 1.** XDP of $In_{16}Fe_8S_{32}$ and the proposed Rietveld refinement.

(16*c* and 16*d*) sites. The sites with negligible occupancy after each refinement were rejected for further analysis. For example, for the sample with 0.7 Li/mol, the occupancy of the 48*f* site obtained after the first refinement was below the experimental error and this site was not considered further in the analysis. In a second fitting (now without the 48*f* site),

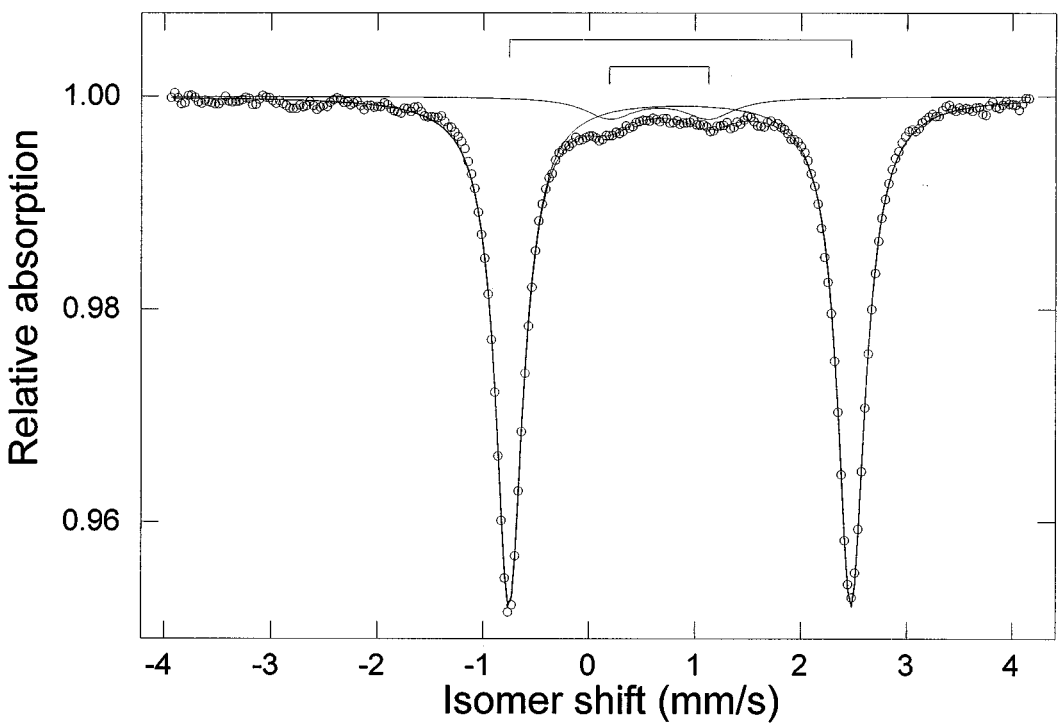


**FIG. 2.** $^{57}Fe$ Mössbauer spectrum of $In_{16}Fe_8S_{32}$.

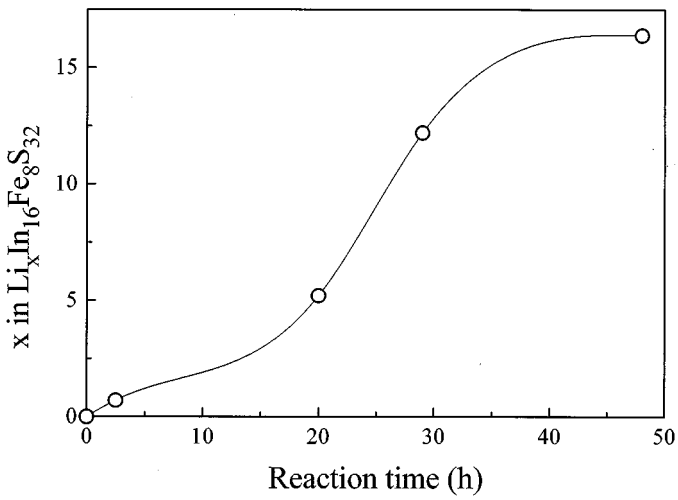


**FIG. 3.** Amount of inserted lithium as a function of reaction time.

the occupancy of Fe atoms in the 16*c* site was 0.06 ± 0.07. As the value of the standard deviation was higher than the occupancy value, this site was also discarded. In a third fitting, the occupancy of Fe on the 8*b* site was 0.07 ± 0.08. For the same reasons, this site was also eliminated. Table 3 shows the values obtained after each fitting. A similar procedure was carried out for all the samples. Concerning the peaks of the Parafilm (P in Fig. 4), they were included in the fitting as background.

*(b.1)* $Li_{0.7}In_{16}Fe_8S_{32}$. The Rietveld refinement of XDP is shown in Fig. 4a. A line broadening of the diffraction peaks and some significant changes in the relative intensities of the reflections were observed. The first effect is a consequence of a weak loss of long-range order induced by lithium insertion in the rigid three-dimensional host lattice. The changes observed in line intensity can be ascribed to the variations in site occupancy as a result of cation migration during the lithium insertion process (vide infra).

The unit cell parameter, cation distribution, and *R* values obtained from Rietveld analysis are included in Table 4. Little changes in the unit cell were observed after 0.7 Li insertion (0.07%), which can be considered to be within the experimental errors during the recording of the XDP. The main effect induced by the insertion of lithium is a new cation distribution, which can be considered to be a consequence of the migration of first, In atoms from 8*a* and 16*d* sites toward vacant 8*b* and 16*c* sites, and second, Fe atoms from octahedral 16*d* sites toward tetrahedral 8*a* sites. Preceding works have shown that indium atom migration can be observed in copper thiospinels during lithium insertion (4) in a way similar to that observed in our case. An additional effect consists in the increase of the value of *x* (position of S atoms), ≈1%, which lets the framework remain almost intact and accommodate the cations in the new occupied sites.

The $^{57}$Fe Mössbauer spectrum of $Li_{0.7}In_{16}Fe_8S_{32}$ is shown in Fig. 5a, and the corresponding hyperfine parameters are listed in Table 5. The subspectrum corresponding to the 16*d* site does not show any important variation in the hyperfine parameters after intercalation: the isomer shift $\delta$ and the linewidth $\Gamma$ vary slightly. These results show that the 16*d* sites remain basically unaltered during the first steps of lithium insertion. On the contrary, the relative area as referred to the area of the signal caused by atoms in the 8*a* site decreases significantly. For this second site, the parameters are similar to those observed for the pristine compound and only a weak increase of the linewidth was observed. This effect is more important for the sample with $x = 5.2$ and it will be discussed in the next section. Finally, Table 6 includes the Fe distribution obtained from relative areas of the signals in the Mössbauer spectrum. These results can be compared with the distribution obtained from the Rietveld analysis (Tables 1 and 4). Both techniques are coincident in evidencing low-extension migration of Fe atoms from octahedral 16*d* to tetrahedral 8*a* sites after intercalation of 0.7 Li/mol.

*(b.2)* $Li_{5.2}In_{16}Fe_8S_{32}$. For this sample, the XDP and Rietveld refined profile are included in Figure 4b. A comparison with Figure 4a evidences several changes in the intensity of the Bragg reflections. The $I_{022}/I_{004}$ ratio that was lower than 1 for 0.7 Li is now greater than unity and the

**TABLE 3**
**Cation Distribution for the Successive Fittings of the XDP of the Chemically Lithiated Sample $Li_{0.7}In_{16}Fe_8S_{32}$**

| | Second fitting | | Third fitting | | Last fitting | | |
|---|---|---|---|---|---|---|---|
| Site | In ± 0.02 | Fe ± 0.07 | In ± 0.02 | Fe ± 0.08 | In ± 0.02 | Fe ± 0.12 | Total |
| 8*a* | 6.96 | 0.97 | 6.93 | 1.12 | 6.91 | 1.09 | 8.00 |
| 8*b* | 0.12 | 0.11 | 0.15 | 0.07 | 0.32 | | 0.32 |
| 16*c* | 0.12 | 0.06 | 0.18 | | 0.19 | | 0.19 |
| 16*d* | 8.80 | 6.86 | 8.75 | 6.80 | 8.59 | 6.91 | 15.50 |
| Total | 16.00 | 8.00 | 16.00 | 8.00 | 16.00 | 8.00 | 24.00 |

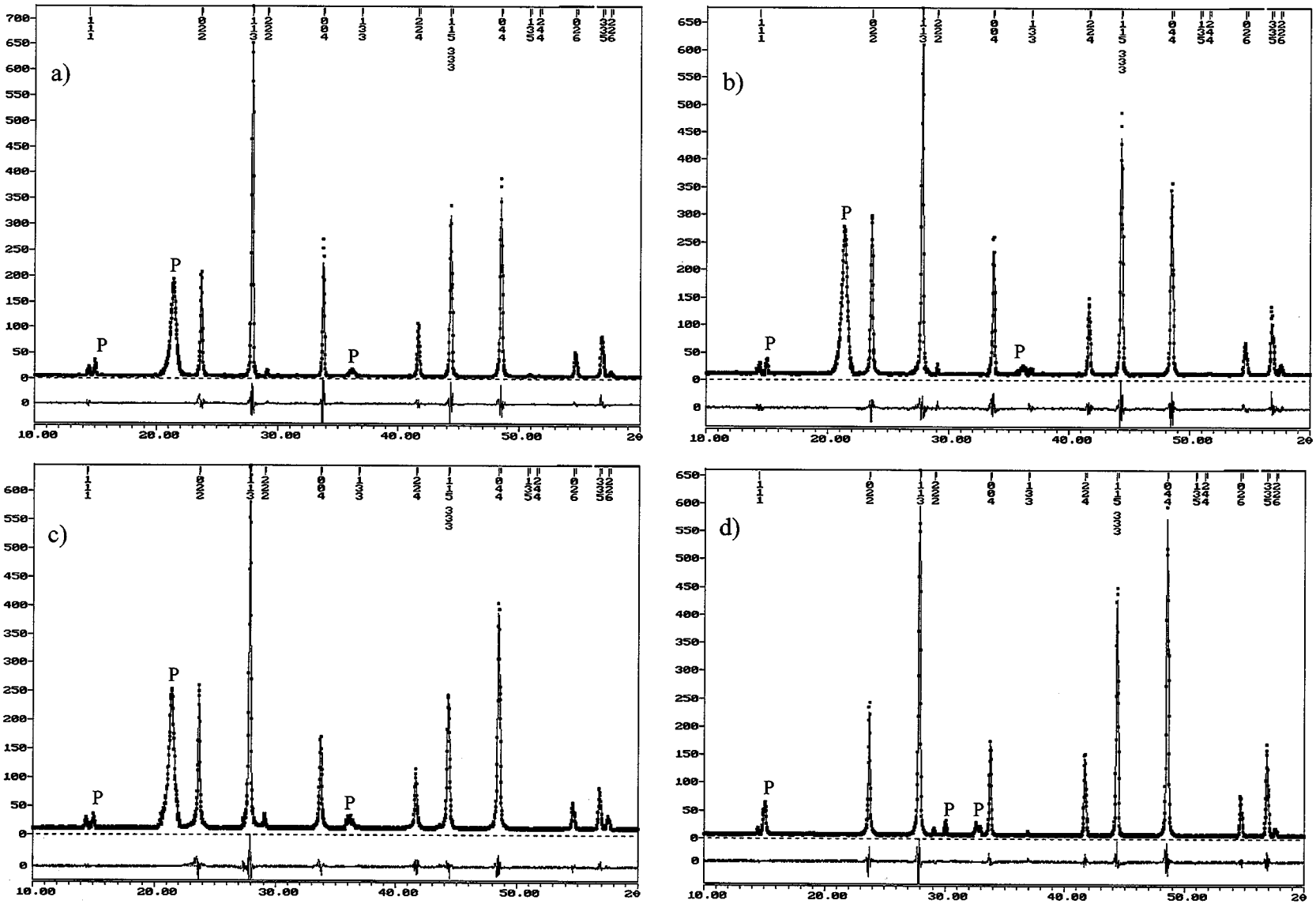


**FIG. 4.** XDP and the Rietveld refinement of $Li_xIn_{16}Fe_8S_{32}$: (a) $x = 0.7$; (b) $x = 5.2$; (c) $x = 12.2$; (d) $x = 16.4$ (peaks coming from Parafilm are marked P).

**TABLE 4**

**Results of Rietveld Analyses of XDP Data of $Li_{0.7}In_{16}Fe_8S_{32}$, $Li_{5.2}In_{16}Fe_8S_{32}$, $Li_{12.2}In_{16}Fe_8S_{32}$, and $Li_{16.4}In_{16}Fe_8S_{32}$ According to the Space Group $Fd\bar{3}m$, Origin 2: 8*a* (1/8, 1/8, 1/8), 8*b*(3/8, 3/8, 3/8), 16*c*(0, 0, 0), 16*d*(1/2, 1/2, 1/2), and 32*e*(*x*, *x*, *x*)**

$Li_{0.7}In_{16}Fe_8S_{32}$: $a = 10.6152(3)$ Å, $x = 0.2593(4)$

| | Occupancy | | | | | |
|---|---|---|---|---|---|---|
| Site | In | Fe | Li | S | Total | Correlation factors |
| 8*a* ($T_d$) | 6.91(2) | 1.09(12) | | | 8.00 | $R_p = 8.58$ |
| 8*b* ($T_d$) | 0.32(2) | | | | 0.32 | $wR_p = 12.32$ |
| 16*c* ($O_h$) | 0.18(2) | | 0.70 | | 0.88 | $R_{expected} = 6.96$ |
| 16*d* ($O_h$) | 8.59(2) | 6.91(12) | | | 15.50 | $S = 1.77$ |
| 32*e* | | | | 32.00 | 32.00 | $R_{Bragg} = 2.77$ |

$Li_{5.2}In_{16}Fe_8S_{32}$: $a = 10.6107(3)$ Å, $x = 0.2673(4)$

| | Occupancy | | | | | |
|---|---|---|---|---|---|---|
| Site | In | Fe | Li | S | Total | Correlation factors |
| 8*a* ($T_d$) | 6.25(4) | 1.10(4) | | | 7.35 | $R_p = 7.63$ |
| 8*b* ($T_d$) | 0.71(4) | 0.54(4) | | | 1.25 | $wR_p = 10.41$ |
| 16*c* ($O_h$) | 2.09(4) | | 5.20 | | 7.29 | $R_{expected} = 5.90$ |
| 16*d* ($O_h$) | 6.95(4) | 6.36(4) | | | 13.31 | $S = 1.76$ |
| 32*e* | | | | 32.00 | 32.00 | $R_{Bragg} = 2.29$ |

$Li_{12.2}In_{16}Fe_8S_{32}$: $a = 10.6131(3)$ Å, $x = 0.2624(4)$

| | Occupancy | | | | | |
|---|---|---|---|---|---|---|
| Site | In | Fe | Li | S | Total | Correlation factors |
| 8*a* ($T_d$) | 6.52(4) | 1.05(5) | | | 7.57 | $R_p = 6.74$ |
| 8*b* ($T_d$) | 0.28(4) | 0.98(5) | | | 1.26 | $wR_p = 9.20$ |
| 16*c* ($O_h$) | 0.07(4) | 0.30(5) | 12.20 | | 12.57 | $R_{expected} = 5.93$ |
| 16*d* ($O_h$) | 9.13(4) | 5.67(5) | | | 14.80 | $S = 1.55$ |
| 32*e* | | | | 32.00 | 32.00 | $R_{Bragg} = 2.52$ |

$Li_{16.4}In_{16}Fe_8S_{32}$: $a = 10.6082(3)$ Å, $x = 0.2541(4)$

| | Occupancy | | | | | |
|---|---|---|---|---|---|---|
| Site | In | Fe | Li | S | Total | Correlation factors |
| 8*a* ($T_d$) | 5.56(6) | 2.38(7) | | | 7.94 | $R_p = 7.18$ |
| 8*b* ($T_d$) | | 0.89(7) | | | 0.89 | $wR_p = 10.31$ |
| 16*c* ($O_h$) | 0.11(6) | 1.21(7) | 14.6(2) | | 15.92 | $R_{expected} = 5.65$ |
| 16*d* ($O_h$) | 10.43(6) | 3.52(7) | 1.8(2) | | 15.75 | $S = 1.81$ |
| 32*e* | | | | 32.00 | | $R_{Bragg} = 1.77$ |

intensities of the (115, 333) and (335) reflections have increased significantly. These modifications in the intensities are indicative of further changes in the cation distribution. The Rietveld analysis showed that the occupancy of the 8*a* and especially the 16*d* sites has decreased. On the other hand, an increase of the occupancy was detected for the 8*b* sites and again especially for the octahedral 16*c* site. Table 4 includes the cation distribution of this sample.

Concerning In atoms, a migration from the 8*a* and 16*d* sites toward the 8*b* and 16*c* sites can be observed when the composition changes from $Li_{0.7}In_{16}Fe_8S_{32}$ to $Li_{5.2}In_{16}Fe_8S_{32}$. Thus, a decrease of 0.66 indium atoms is observed in 8*a* sites, while for the 16*d* sites a more important decrease of 1.64 atoms takes place. Of these 2.3 In atoms displaced from the 8*a* and 16*d* sites, 0.39 move to 8*b* sites and the rest go to 16*c*, which changes its occupancy from 0.18 In for 0.7 Li to 2.09 In for 5.2 Li (Table 4). For Fe atoms, the situation is different, since the 8*a* and 16*c* sites are not affected in the same extension. In fact, the occupancy of 8*a* sites does not change significantly, as the change from 1.09 to 1.10 falls within the tabulated values of standard deviation. On the contrary, a migration of 0.55 atoms from the octahedral 16*d* site toward the tetrahedral 8*b* site is exclusively observed, as no Fe atoms are present in the 16*c* site of $Li_{5.2}In_{16}Fe_8S_{32}$. In conclusion, lithium insertion originates a strong migration from the usually occupied 8*a* and 16*d* sites toward the usually empty 8*b* and 16*c* sites.

The observed cation redistribution does not affect the unit cell parameter *a*, which remains almost constant on lithium insertion. On the contrary, the position of sulfur atoms varies significantly as evidenced by the evolution of the fractional coordinate *x*. Following the same sequence observed for the $Li_{0.7}In_{16}Fe_8S_{32}$ sample, a strong increment of *x* is observed from 0.2569 (pristine sample, Table 1) to 0.2673 (about 4% more, 5.2 Li, Table 4). This increment can be related with the presence of a larger content of heavy cations (Fe and In) in 8*b* sites, which progressively leads to a larger departure from the spinel structure, in which the 8*b* site is empty and $x = 0.25$. In fact, the occupancy of this site is 0 for the pristine sample and it increases to 0.50 for 0.7 Li and to 3.34 for 5.2 Li.

In the Mössbauer spectrum (Fig. 5b), the subspectra corresponding to 16*d* and 8*a* sites were also well resolved. The

**TABLE 5**

**Hyperfine Parameters of Mössbauer Spectra of $Li_xIn_{16}Fe_8S_{32}$: Isomer Shift (IS), Quadrupole Splitting (QS), Full-Width at Half-Maximum (LW), and Relative Area (RA)**

| Site | *x* | IS (mm/s) | QS (mm/s) | LW (mm/s) | RA (%) |
|---|---|---|---|---|---|
| 16*d* ($O_h$) | 0.7 | 0.862(1) | 3.2(1) | 0.261(8) | 92(1) |
| | 5.2 | 0.865(1) | 3.2(1) | 0.259(8) | 82(2) |
| | 12.2 | 0.864(2) | 3.2(1) | 0.294(9) | 70(2) |
| | 16.4 | 0.863(1) | 3.2(1) | 0.242(8) | 51(2) |
| 8*a* ($T_d$) | 0.7 | 0.63(4) | 0.90(5) | 0.67(8) | 8(1) |
| | 5.2 | 0.65(8) | 1.3(1) | 1.0(2) | 12(2) |
| | 12.2 | 0.70(5) | 1.40(9) | 0.8(1) | 14(2) |
| | 16.4 | 0.71(2) | 1.71(7) | 0.82(7) | 24(2) |
| 8*b* ($T_d$) | 0.7 | | | | |
| | 5.2 | 0.34(4) | 0.59(6) | 0.47(9) | 6(2) |
| | 12.2 | 0.25(3) | 0.71(7) | 0.56(6) | 12(2) |
| | 16.4 | 0.32(2) | 0.63(3) | 0.61(5) | 18(2) |
| 16*d* ($O_h$) | 0.7 | | | | |
| | 5.2 | | | | |
| | 12.2 | 0.57(2) | 2.62(8) | 0.29(1) | 4(2) |
| | 16.4 | 0.69(1) | 2.61(8) | 0.25(2) | 7(2) |

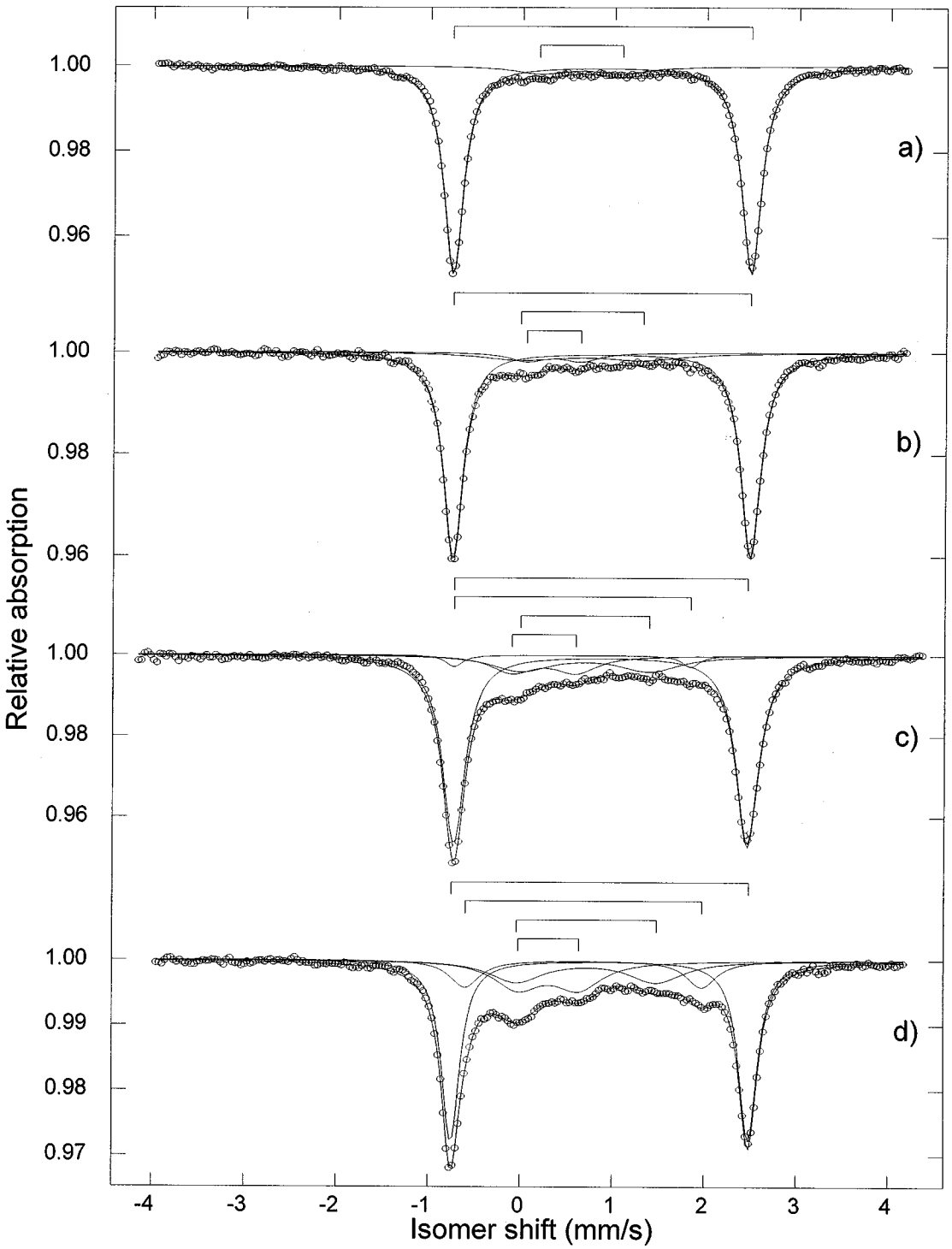


**FIG. 5.** $^{57}$Fe Mössbauer spectra of the lithiated phases $Li_xIn_{16}Fe_8S_{32}$: (a) $x = 0.7$; (b) $x = 5.2$; (c) $x = 12.2$; (d) $x = 16.4$.

hyperfine parameters are included in Table 5. For the 16*d* site, there are no changes either in isomer shift or in quadrupole splitting from $Li_{0.7}In_{16}Fe_8S_{32}$ to $Li_{5.2}In_{16}Fe_8S_{32}$. The increase in the linewidth is negligible according to the values of standard deviation. The relative area varies from 92% (0.7 Li) to 82% (5.2 Li), indicating that some Fe atoms leave the 16*d* site to migrate to other sites.

Concerning the 8*a* site, the Mössbauer parameters show little change, particularly in the values of the isomer shift. A weak but nonnegligible increase in the quadrupole

**TABLE 6**
**Cation Distribution of Fe Atoms Calculated from Mössbauer Data**

| | $x$ in $Li_xIn_{16}Fe_8S_{32}$ | | | | |
|---|---|---|---|---|---|
| Site | 0 | 0.7 | 5.2 | 12.2 | 16.4 |
| 8*a* ($T_d$) | 0.56 | 0.64(8) | 0.96(16) | 1.12(16) | 1.92(16) |
| 8*b* ($T_d$) | | | 0.48(16) | 0.96(16) | 1.44(16) |
| 16*c* ($O_h$) | | | | 0.32(16) | 0.56(16) |
| 16*d* ($O_h$) | 7.44 | 7.36(8) | 6.56(16) | 5.60(16) | 4.08(16) |

splitting and the linewidth indicate that the distortion increases and the symmetry of the charge distribution decreases, respectively. According to earlier works (11, 13), these effects can be associated with the presence of several tetrahedral environments. If some of the adjacent positions are vacant, the surrounding atoms are displaced somewhat toward the vacancy, which leads to a decrease in the symmetry of the occupied positions. This distortion is revealed by Mössbauer spectroscopy as an increased quadrupole splitting of the subspectrum of the $^{57}$Fe atom in a tetrahedral coordination. Further effects result from the random occupation of octahedral sites by Fe and In, having different ionic radii. Because of the different possibilities of the vacancy and cation distribution around Fe atoms in tetrahedral sites, these Fe atoms are not completely equivalent, thus leading to an increase of the linewidth. The influence of vacancies on the Mössbauer spectrum of octahedrally coordinated Fe atoms is less evident. The main contribution to the quadrupole splitting of about 3.2 mm/s in the case of these compounds comes from a trigonal distortion of the sulfur octahedron (14). Such a distortion is frequently observed in spinels and is due to the fact that most of the cations are too large to be accommodated on tetrahedral sites, so that they originate some displacement of the anions, distorting at the same time the octahedral sites. This distortion splits the $t_{2g}$ orbitals into a singlet and a doublet, creating an asymmetric charge distribution, and giving the main contribution to the observed quadrupole splitting (14). Additional distortions caused by tetrahedral vacancies may slightly increase or decrease this splitting but its order of magnitude does not change.

In addition, a third subspectrum with a significantly lower isomer shift was resolved in the Mössbauer spectrum of Fig. 5b, which describes a further tetrahedral environment of Fe atoms. A comparison between Mössbauer and Rietveld results allowed us to conclude that this subspectrum can be ascribed to the iron atoms in 8*b* sites of the spinel structure. The values of quadrupole splitting and linewidth are clearly lower than those of the 8*a* site. A first argument to explain this phenomenon is the lower occupancy of 8*b* sites as compared with 8*a* sites. Another argument concerns the distribution of cations and vacancies around each site. In fact, atoms placed in 48*f* sites are the first cationic neighbors of 8*a* and 8*b* sites. Since the 48*f* sites are empty, we have to pay attention to the second cationic neighbors. Thus, for atoms placed in the 8*a* site, the neighbors are the atoms in 16*c*. The occupancy of this site leads to a larger number of different possibilities of distributions than in 16*d*, because there are more vacancies (about 50%) and three different atoms (Li, In, and Fe). Therefore the effect of the distribution is stronger. On the contrary, for the atoms placed in the 8*b* sites, the neighbors are in 16*d* sites, where only 1/6 of the vacancies are present and only two different atoms (In and Fe) occupy these sites. The effect of this situation on the linewidth and quadrupole splitting is not as marked as in the 8*a* sites.

Finally, the value of the isomer shift for the 8*b* site is lower than that for the 8*a* site. This indicates a decrease of the ioncity of the Fe–S bond and will be discussed in the next section.

*(b.3)* $Li_{12.2}In_{16}Fe_8S_{32}$. Figure 4c shows the XDP and the proposed calculated profile with the Rietveld refined parameters which are included in Table 4. A noteworthy effect is again the decrease of the intensity of the (044), (333, 115), and (335) reflections, as a result of new cation migrations. The most important redistribution affects indium atoms in the 16*c* and 16*d* sites. The occupancy of the former decreases from 2.09 (for $Li_{5.2}In_{16}Fe_8S_{32}$) to 0.07 (for $Li_{12.2}In_{16}Fe_8S_{32}$), while the 16*d* sites increase their occupancy from 6.95 to 9.13. In addition, a decrease in 8*b* site occupancy is observed, which also contributes to the larger content of indium atoms in both the 8*a* and 16*d* sites. Concerning iron atoms, first it is worth noting that the 16*c* sites, which were only occupied by indium atoms in previous compositions, now contain a significant amount of iron. In addition, the occupancy decreases for 16*d* sites, increases for 8*b* sites, and remains almost constant for 8*a* sites. Globally, the evolution of site occupancy makes the cation distribution of $Li_{12.2}In_{16}Fe_8S_{32}$ closer to that observed in the pristine spinel situation, with the stronger scatterers in the 8*a* and 16*d* sites. Finally, the value of $x$ (coordinate of S atoms) decreases, in good agreement with the trend toward the initial cation distribution.

The Mössbauer spectrum and hyperfine parameters are included in Fig. 5c and Table 5, respectively. We find here the same subspectra described earlier for the sample having 5.2 Li, with the same characteristics and ascribable to the 8*a*, 8*b*, and 16*d* sites. A fourth subspectrum is observed, with hyperfine parameters which are nearer to those of an octahedral site, and thus can be ascribed to 16*c*. The good agreement between the Mössbauer results and the Rietveld analysis confirms this assignment.

The isomer shift of the 16*c* site, 0.57 mm/s, is lower than that of the 16*d* site, 0.86 mm/s. A similar difference can be observed for the tetrahedral sites: 0.25 mm/s for the 8*b* site and 0.70 mm/s for the 8*a* site. The lower values of the isomer shift are observed in the sites that increase their occupancy with lithium insertion. Since $\Delta R/R$ is negative for $^{57}$Fe, low isomer shifts are originated by an increase in the electronic density at the nucleus. This in turn may take place by three different mechanisms:

(i) directly, by transferrring two electrons to the Fe atom, with a neat reduction from $Fe^{2+}$ to $Fe^0$, which results in a larger electronic density of the *s* orbital.

(ii) by an indirect mechanism, decreasing the electronic density of the *d* orbital and thus the shielding effect. This is the case of the oxidation from $Fe^{2+}$ to $Fe^{3+}$.

(iii) by changes in the covalencey. For a given oxidation state, the value of $\delta$ depends on the nature and on the electronegativity of the ligands. A decrease of the electronegativity of an Fe–S bond causes the ionic character of the bond to decrease and the electronic density of the valence band to increase.

The second mechanism can be directly neglected, as lithium insertion is accompanied by electron donation to the host lattice. Moreover, since no bands ascribable to $Fe^0$ are observed, the first mechanism can also be neglected. Thus, we can conclude that the effect of the lithium insertion is not a clear reduction of Fe atoms but an increase in the covalency of the Fe–S bonds, which affect mainly the electron density at the nucleus of atoms in sites which are unoccupied in the pristine host solid (8*b* and 16*c* sites).

*(b.4)* $Li_{16.4}In_{16}Fe_8S_{32}$. Finally, the XDP of $Li_{16.4}In_{16}Fe_8S_{32}$ shows strong modifications in the intensities, especially concerning the (333, 155) and (044) Bragg reflections (see Fig. 4d). In fact, the Rietveld refinement shows important changes in the occupancy of the different sites (Table 4). Indium atoms move from 8*a* and 8*b* (which become unoccupied by In atoms) toward the 16*d* site, the 16*c* site being almost not involved. For Fe atoms, the situation is just the opposite, since they move from 16*d* toward the 16*c* and 8*a* sites. Now the 8*b* site is not involved in the migration process. Furthermore, the value of *x* (position of S atoms) decreases below the obtained value for the pristine compound, close to the theoretical value for a cubic close-packed structure, 0.25. This means that the anion array is less distorted for high lithium amounts.

Concerning the Mössbauer spectrum, shown in Fig. 5d, the four subspectra attributed the 8*a*, 8*b*, 16*c*, and 16*d* sites are again present. The changes in the relative areas evidence the migrations of the Fe atoms from the 16*d* site toward the other sites as observed by the Rietveld results.

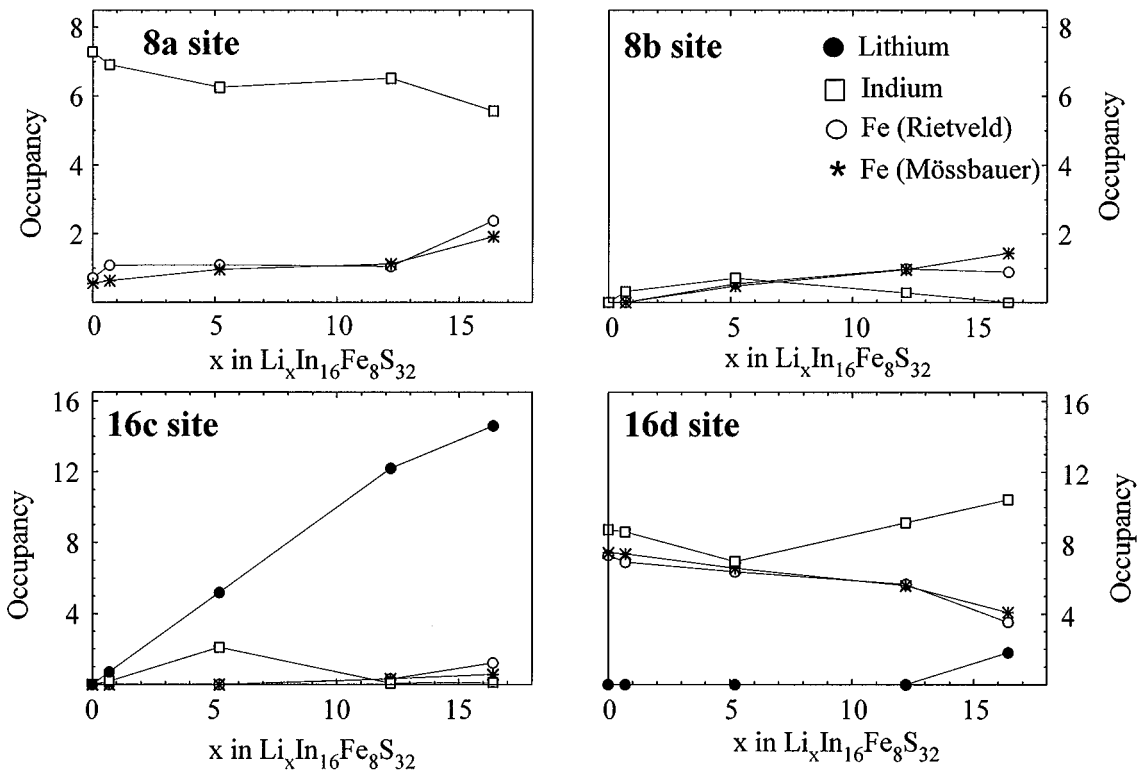


**FIG. 6.** Evolution of the occupancy of the 8*a*, 8*b*, 16*c*, and 16*d* sites as a function of the lithium content.

## CONCLUSION

Taking into account the results of the present study obtained by Rietveld and Mössbauer analysis, we can conclude that during the intercalation reaction there is not a net expansion of the cell. The framework accomodates the inserted ions in two ways:

(a) cation migrations. Lithium intercalation leads to a net migration of In atoms from the 8*a* site toward the 16*d* site whereas Fe atoms take the opposite way (from 16*d* to 8*a*). Thus, concerning the In and Fe atoms in these two sites, the lithium intercalation seems to originate a tendency toward a normal spinel structure. A preliminary study concerning the electrochemical lithiation of some thiospinels (including $In_{16}Fe_8S_{32}$) by Mössbauer spectroscopy has reported a similar migration effect (15). Moreover, other minor effects are observed: a weak occupancy of the 8*b* and 16*c* sites takes place. It is worth noting the high occupancy of In atoms in 16*c* for the sample with 5.2 Li ($\approx 2.1$) compared to the other samples ($< 0.20$) . Figure 6 summarizes the evolution of the In (obtained from the Rietveld refinement) and Fe (from Rietveld and Mössbauer analysis) distribution in the different sites as a function of the inserted lithium.

(b) a variation in the position on the sulfur atoms. Small quantities of lithium originate an increase of the $x$ value, moving the S atoms away from the theoretical position for a cubic close-packed structure and distorting the coordination polyhedra. For large amounts of lithium, the value of $x$ decreases, coming close to the theoretical one and decreasing the distortion of the sulfur polyhedra.

(c) the lithium insertion does not induce a clear reduction of $Fe^{2+}$ ions. The values of isomer shift of the new occupied positions (8*b* and 16*c*) indicate a decrease in the ionic character of the Fe–S bonds. Thus, the Mössbauer results show that the electrons are absorbed by the framework, increasing the covalency of the structure.

## ACKNOWLEDGMENTS

The authors are indebted to the European community, the Ministries of Foreign Office (France) and Education (Spain), for financial support (Contact JOU2-CR93-026, Human Capital and Mobility No. ERBCHBGCT 93.0430, Training and Mobility of Researchers No. ERBFMBICT 96.0768, and the PICASSO program).

## REFERENCES

1. M. Eisenberg, *J. Electrochem. Soc.* **127,** 2382 (1980).
2. A. C. W. P. James, B. Ellis, and J. B. Goodenough, *Solid State Ionics* **27,** 45 (1988).
3. M. Pernet, P. Strobel, B. Bonnet, and P. Bordet, *Solid State Ionics* **66,** 259 (1993).
4. J. Morales, J. L. Tirado, M. L. Elidrissi Moubtassim, J. Olivier-Fourcade, and J. C. Jumas, *J. Alloys Compd.* **217,** 176 (1995).
5. M. A. Cochez, J. C. Jumas, P. Lavela, J. Morales, J. Olivier-Fourcade, and J. L. Tirado, *J. Power Sources* **62,** 99 (1996).
6. M. L. Elidrissi Moubtassim, J. Olivier-Fourcade, J. Senegas, and J. C. Jumas, *Mater. Res. Bull.* **28,** 1083 (1993).
7. A. F. Wells, "Structural Inorganic Chemistry," 4th ed., p. 491. Clarendon Press, Oxford, U.K., 1975.
8. R. J. Hill, J. R. Craig, and G. V. Gibbs, *J. Phys. Chem. Solids* **39,** 1105 (1978).
9. D. B. Wiles, and R. A. Young, *J. Appl. Crystallogr.* **28,** 366 (1995).
10. W. Kündig, *Nucl. Instrum. Methods* **75,** 336 (1969).
11. M. Womes, J. Olivier-Fourcade, J. C. Jumas, F. Aubertin, and U. Gonser, *J. Solid State Chem.* **97,** 249 (1992).
12. H. D. Lutz and M. Jung, *Z. Anorg. Allg. Chem.* **57,** 579 (1989).
13. M. Womes, F. Py, M. L. Elidrissi Moubtassim, J. C. Jumas, J. Olivier-Fourcade, F. Aubertin, and U. Gonser, *J. Phys. Chem. Solids* **55** (11), 1323 (1994).
14. M. Eibschütz, E. Hernon, and S. Shtrikman, *Solid State Commun.* **5,** 529 (1967).
15. A. Krämer, M. L. Elidrissi Moubtassim, C. Bousquet, J. Olivier-Fourcade, J. C. Jumas, and J. L. Tirado, *Nuovo Cimento D* **18** (2–3), 237 (1996).